INTERNATIONAL JOURNAL FOR NUMERICAL METHODS IN FLUIDS, VOL. 22, 731–754 (1996)

A CHARACTERISTIC-LIKE METHOD FOR THERMALLY EXPANDABLE FLOW ON UNSTRUCTURED TRIANGULAR GRIDS

C. A. HALL AND T. A. PORSCHING

Department of Mathematics and Statistics, University of Pittsburgh, Pittsburgh, PA 15260, U.S.A.

SUMMARY

Finite-difference-like discretizations are developed for the time-dependent Navier–Stokes equations and the thermal energy equation on Delaunay triangulations of the flow domain. The flow is assumed to be thermally expandable; that is, the density varies only with temperature. A characteristic-like (CL) method is used to discretize the temporal and convective terms. The dual variable method reduces the size of the discrete system by a factor of five.

KEY WORDS: thermally expandable flow; covolume method; characteristic curve; Delaunay tessellation; dual variable method

1. INTRODUCTION

The finite volume or covolume method for generating finite difference equations was studied in Reference 1 for the heat equation and in References 2–8 for the incompressible Navier–Stokes equations. In References 9 and 10 the authors combined and extended these approaches to discretize a thermally expandable two-phase flow model. See Reference 11 for a current review of the literature on covolume methods in computational fluid dynamics. In this paper we consider thermally expandable flow with conduction and introduce a new covolume approach, based on the idea of characteristics, for the discretization of the convection term of the energy and momentum equations.

The equation system that we consider consists of the *continuity equation*

$$\frac{\partial \rho}{\partial t} + \nabla \cdot (\rho \mathbf{q}) = 0, \tag{1}$$

the *momentum equation*

$$\frac{\partial (\rho \mathbf{q})}{\partial t} + \nabla \cdot (\rho \mathbf{q}\mathbf{q}^{\mathrm{T}}) - \mu \Delta \mathbf{q} = -\nabla p + \mathbf{f}, \tag{2}$$

the *thermal energy equation**

$$c_{\mathrm{p}} \frac{\partial (\rho T)}{\partial t} + c_{\mathrm{p}} \nabla \cdot (\rho \mathbf{q} T) - \nabla \cdot k \nabla T = Q \tag{3}$$

and a thermally expandable[29] *equation of state*, e.g.

$$\rho(T) = \frac{Rmp^*}{T}, \tag{4}$$

CCC 0271–2091/96/080731–24

Received 2 September 1994
Revised 5 July 1995

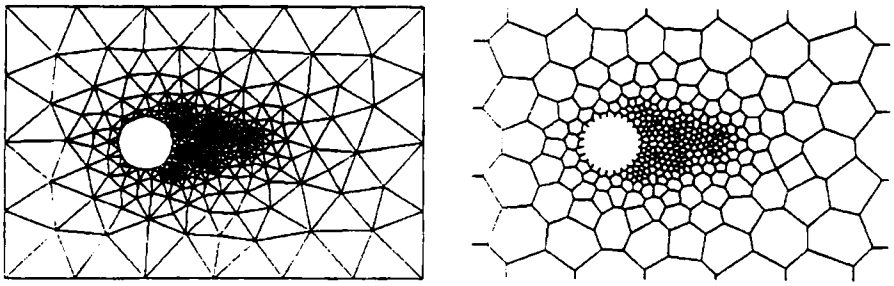

Figure 1. Delaunay and Voronoi tessellations

where ρ is the density, $\mathbf{q} = (q_1, q_2)$ is the velocity, p is the pressure, T is the temperature, $\mathbf{f}$ is the body force, Q is the heat source, μ is the viscosity, c_p is the specific heat, k is the thermal conductivity, R is the gas constant, m is the molecular weight, p^* is the constant system pressure and t is the time.

[The approach discussed here could just as easily be applied to a system in which the energy equation is given in terms of fluid enthalpy as

$$\frac{\partial(\rho H)}{\partial t} + \nabla \cdot (\rho \mathbf{q} H) = Q. \tag{3a}$$

As studied in References 10 and 12, the state equation (4) is replaced by

$$\rho = \rho(H, p^*) \tag{4a}$$

and involves interpolation of tabulated data.]

We assume that (1)–(4) hold in a flow domain Ω whose boundary $\partial\Omega$ is polygonal and which has been decomposed into triangular flow cells. On each segment of the boundary $\partial\Omega$ we assume that either a temperature is given or the adiabatic condition holds. The fluid boundary conditions are that either the velocity $\mathbf{q}$ is given or the pressure p and tangential component of $\mathbf{q}$ are given.

A geometric construction which has proven useful for generating finite element and finite volume discretizations of planar or solid regions into well-proportioned triangular or tetrahedral simplices is the so-called *Delaunay triangulation* and its dual the Voronoi tessellation. What makes the Delaunay triangulation popular is that (i) there are very efficient algorithms for computing it[14,15] and (ii) it produces triangles that are as close to equilateral as possible[15] for a given set of points. See Figure 1 for an example of Delaunay triangulation and the associated Voronoi tessellation.

One of the primary advantages of basing the discretization of boundry value problems on Delaunay/Voronoi constructions is the ability to easily define dual control volume partitions that can be locally graded or refined[16] and which are mutually orthogonal. Local grading permits efficient resolution and control of spatial discretization errors, while orthogonal control volumes produce small discrete systems (especially when combined with the dual variable method (DVM) of reducing system dimensionality) and improved treatment of flow boundary conditions. A main objective of References 2–5 and 9 and the current work has been to link efficient control volume generation with complementary volume flow discretization and the DVM to produce an approach capable of delivering accurate approximations from computational models that are comparatively small in size. Finally, if (for example) the reverse Cuthill–McKee algorithm is used to order the triangles and vertices of the triangles in a Delaunay triangulation, the system representing the discrete form of equations (1)–(3) will have a small bandwidth and profile.

For a single space variable x the notion of *characteristics* or *characteristic curves* of a first-order hyperbolic partial differential system

$$\mathbf{u}_t + A\mathbf{u}_x = f, \quad A \in \mathbb{R}^{n \times n}, \tag{5}$$

has been the basis for various numerical methods for approximating their solutions; see Reference 17 for a discussion. The basic idea is to transform the system (5) into a system of the generic form

$$\mathbf{v}_i^{\mathrm{T}} \frac{\mathrm{d}\mathbf{u}}{\mathrm{d}t} = g_i, \quad i = 1, 2, \cdots, n, \tag{6}$$

each member of which holds along a *characteristic curve* $x_i(t)$ satisfying

$$\frac{\mathrm{d}x_i}{\mathrm{d}t} = \lambda_i(x, t, \mathbf{u}(x, t)), \quad i = 1, 2, \cdots, n, \tag{7}$$

where λ_i is an eigenvalue of A with associated left eigenvector $\mathbf{v}_i$. Discretization of the total derivative in (7) at time level t_{m+1} proceeds by integrating the characteristic equations (7) backwards to time level t_m. This provides a location $x_i(t_m)$ which is then used in the discretization of (6). The use of characteristics in the numerical solution of scalar hyperbolic equations is not new; see References 7, 17 and 18 and references cited therein. However, in Sections 2 and 3 we use this same general approach and the fact that in the covolume method the vector equation (2) is replaced by a scalar equation to discretize only certain terms in the entire flow model (1)–(4).

2. FINITE VOLUME DISCRETIZATION OF ENERGY EQUATION

MacNeal[1] developed finite difference equations for the discretization of the heat conduction equation on triangular grids. The temperature unknowns are associated with triangle circumcentres. The authors built upon this work in References 2, 9 and 10 and investigated several approaches to handling the discretization of the convection terms in (2) and (3). These finite volume discretizations included centred difference and donor-cell-type approximations. In this section we present a method for the treatment of the hyperbolic part of (3) that is related to the backward characteristic technique discussed in Section 1. Since there are two space variables, the analogue of the characteristic curve (7) is the *characteristic surface* S given implicitly by the equation $\phi(x, y, t) = 0$, where

$$\frac{\partial \phi}{\partial t} + \nabla \cdot (\mathbf{q}\phi) = 0.$$

For numerical purposes S is not as useful as the so-called *bicharacteristic curves* $\mathbf{r}(t)$ lying on S. They are defined as solutions of the differential equation $\mathrm{d}\mathbf{r}/\mathrm{d}t = \mathbf{q}$. In view of the connection with the underlying notion of characteristics, we say that the method is 'characteristic-like' (CL) and refer to it as the CL method.

Note that $\mathbf{r}(t)$ can be interpreted as a fluid particle path or equivalently as the definition of the Lagrange co-ordinates of a particle. However, we do not regard the CL method as a Lagrangian 'particle-tracking' scheme, since the fundamental quantities determined by the method are associated with a spatially fixed (i.e. Eulerian) grid.

Consider the path $\mathbf{r}_\sigma = (x(t), y(t))$ followed by a fluid particle through the circumcentre (x_σ, y_σ) of triangle σ. Then $\mathbf{q} = (\dot{x}, \dot{y})$ is the velocity of the particle and we note that the total derivative* of the temperature $T(x, y, t)$ along the path $\mathbf{r}_\sigma$ is

$$\frac{\mathrm{d}T}{\mathrm{d}t} = \nabla T \cdot \mathbf{q} + \frac{\partial T}{\partial t}. \tag{8}$$

* The use of total or material derivatives in covolume discretizations of the vorticity transport equation was suggested, though not pursued, by Nicolaides.[7] Classical finite difference schemes utilizing characteristics go back to Courant *et al.*[19] For finite element schemes see e.g. References 18 and 20.

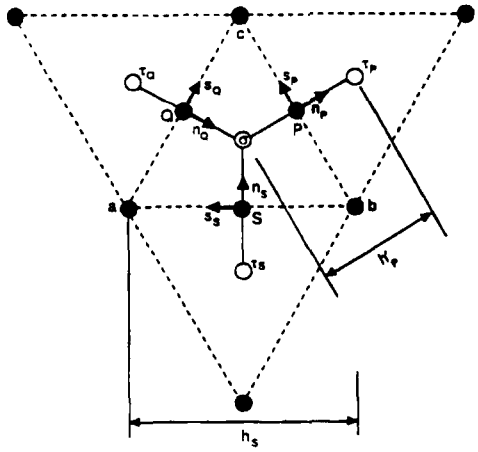

Figure 2. Triangle σ

Hence, recalling that $\partial\rho/\partial t = -\nabla \cdot (\rho \mathbf{q})$, we have from (8) that

$$\rho c_p \frac{dT}{dt} = \rho c_p \left(\nabla T \cdot \mathbf{q} + \frac{\partial T}{\partial t} \right)$$

$$= \rho c_p \frac{\partial T}{\partial t} + c_p [\nabla \cdot (\rho \mathbf{q} T) - T \nabla \cdot (\rho \mathbf{q})]$$

$$= c_p \frac{\partial (\rho T)}{\partial t} + c_p \nabla \cdot (\rho \mathbf{q} T). \tag{9}$$

This can be used to rewrite (3) as

$$\rho c_p \frac{dT}{dt} - \nabla \cdot k \nabla T = Q \tag{10}$$

along the path $\mathbf{r}_\sigma$.

We assign a local Cartesian co-ordinate system ($\mathbf{n}_P$, $\mathbf{s}_P$) to the midpoint P of each side of the triangular grid. The triangle σ in Figure 2 has area A_σ and boundary $\partial\sigma$. The unit normal on $\partial\sigma$ is N. The length of side I is h_I and h_I' is the distance between triangle circumcentres σ and τ_I on the perpendicular bisector through side I. Note that $\mathbf{N} \cdot \mathbf{n}_I = \pm 1$ as $\mathbf{n}_I$ is an outward or inward normal to side I. For each of the N_T-triangles in the triangulation the density ρ_σ, pressure P_σ and temperature T_σ are associated with the circumcentre of triangle σ. For each of the N_S triangle sides the midside normal velocity $\mathbf{q} \cdot \mathbf{n}_I$ is associated with the midpoint of side I.

Recall that the derivative term dT/dt in (10) is the time derivative along the curve $\mathbf{r}_0 = (x(t), y(t))$. Let $t_{m+1} = t_m + \Delta t_m$ be the current value of time t. Assuming that the velocity $q(x, y, t_m)$, density $\rho(x, y, t_m)$ and temperature $T(x, y, t_m)$ are known, the time derivative in (10) at the circumcentre of triangle σ is approximated by (see Figure 3)

$$\frac{dT_\sigma}{dt} \approx \frac{T(x_\sigma, y_\sigma, t_{m+1}) - T(x(t_m), y(t_m), t_m)}{\Delta t_m}. \tag{11}$$

The conduction term in (10) is approximated at σ by area averaging,

$$(\nabla \cdot k \nabla T)_\sigma \approx \int_\sigma \nabla \cdot (k \nabla T)\, dA / A_\sigma, \tag{12}$$

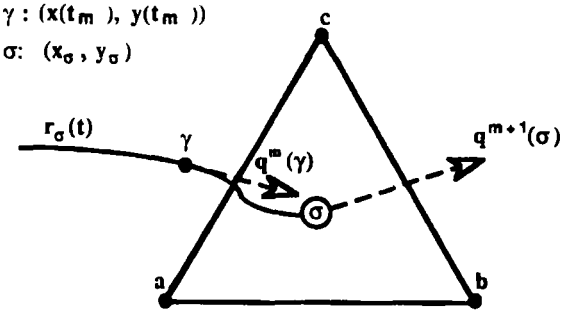

Figure 3. Particle curve through circumcentre of triangle σ

where by the divergence theorem

$$\int_\sigma \nabla \cdot (k\nabla T)\,\mathrm{d}A = \int_{\partial\sigma} k\nabla T \cdot \mathbf{N}\,\mathrm{d}s \approx \sum_{I=\mathrm{P,Q,S}} k\frac{T_{\tau_I} - T_\sigma}{h'_I} h_I. \tag{13}$$

Finally the source term is approximated by Q_σ, the value at the circumcentre.* Collecting (11)–(13), the discretization of (10) at the circumcentre of triangle σ is taken to be

$$\rho_\sigma c_\mathrm{p} A_\sigma \frac{T_\sigma - T(x(t_m), y(t_m), t_m)}{\Delta t_m} - \sum_{I=\mathrm{P,Q,S}} k\frac{T_{\tau_I} - T_\sigma}{h'_I} h_I = Q_\sigma A_\sigma. \tag{14}$$

The unknowns $\{T_\sigma, T_{\tau_\mathrm{P}}, T_{\tau_\mathrm{Q}}, T_{\tau_\mathrm{S}}\}$ in (14) are associated with time level t_{m+1}.

The problem now reduces to finding where the fluid particle (currently at (x_σ, y_σ)) was at time $t = t_m$. To determine the co-ordinates $(x(t_m), y(t_m))$, we integrate

$$\frac{\mathrm{d}\mathbf{r}}{\mathrm{d}t} = \left[\frac{\mathrm{d}x}{\mathrm{d}t}, \frac{\mathrm{d}y}{\mathrm{d}t}\right] = \mathbf{q}$$

backwards from (x_σ, y_σ) along $\mathbf{r}_\sigma$. This yields

$$\begin{bmatrix} x(t_m) \\ y(t_m) \end{bmatrix} - \begin{bmatrix} x_\sigma \\ y_\sigma \end{bmatrix} = \int_{t_{m+1}}^{t_m} \mathbf{q}(x(t), y(t), t)\,\mathrm{d}t$$
$$\approx -\Delta t_m \mathbf{q}(x(t_m), y(t_m), t_m). \tag{15}$$

Rearranging this relation, we determine $x(t_m)$ and $y(t_m)$ as the solution of the *non-linear* simultaneous equations

$$\begin{aligned} x(t_m) + \Delta t_m q_1(x(t_m), y(t_m), t_m) &= x_\sigma, \\ y(t_m) + \Delta t_m q_2(x(t_m), y(t_m), t_m) &= y_\sigma. \end{aligned} \tag{16}$$

Equation (16) is solved for each circumcentre of the mesh, e.g. using Newton's method. This allows us to evaluate $T(x(t_m), y(t_m), t_m)$ in (14). Substituting the resulting approximation into (14) yields a system of equations

$$K\mathbf{T} = \mathbf{s} \tag{17}$$

to be solved at each time step. In general the matrix K has four non-zero entries per row but is diagonal for pure convection problems.

* For irregular tessellations, where the circumcentre may be outside the triangle, we have used the value at the centroid.

In some problems we have found little difference in the results if $\mathbf{q}(x(t_m), y(t_m), t_m)$ in (15) is replaced by $\mathbf{q}_\sigma$, similarly to the finite element scheme in Reference 18. In other problems this linearization does degrade the solution. A third choice we have investigated is to average these two choices; this corresponds to applying the trapezoidal rule to the integral in (15).

In the Appendix we present a convergence analysis for the CL method applied to the one-dimensional model convection equation

$$\frac{\partial \phi}{\partial t} + \frac{q \partial \phi}{\partial x} = 0,$$

subject to the pure initial condition $\phi(x, 0) = \phi_0(x)$, $-\infty < x < \infty$. We prove that if Φ is the computed approximation of ϕ and if linear interpolation is used to reconstruct $\Phi(x, t)$ from its mesh point values, then for any mesh ratio $\Delta t/h$, where Δt is the time step and h is the spatial mesh gauge, the computed solution is always bounded by the initial data; in other words, the method is unconditionally stable. Regarding the convergence of the method, we deduce the following.

1. Under the usual assumption that the mesh ratio is constant, the method is first-order in h in the sense that the discretization error $\Phi(x, t) - \phi(x, t) = O(h)$.
2. If Δt is fixed (at any value), then $\Phi(x, t) - \phi(x, t) = O(h^2)$, i.e. the method is second-order in h.
3. The discretization error consists only of interpolation errors, i.e. the numerical integration in time is exact. Since these errors accumulate as $\Delta t \to 0$, decreasing the time step while keeping h fixed will generally produce a less accurate numerical solution.

Returning now to the general method, we note that we can exploit the form of (4) to decouple (17) from the fluid dynamics equations at each time step. For a given time step the new time temperatures are approximated by solving (17), the new time densities are calculated from (4) and then the new time velocities and pressures are obtained by discretizing (1) and (2) using the new time densities. This process is repeated for each time step.

Our convergence criterion for Newton's method applied to (16) is that the Euclidean norm of the residual be less than 1 per cent of the Euclidean norm of the position vector $(x(t_m), y(t_m))$. Experience to date shows that Newton's method converges in one or two steps, else it cycles, the latter occurring infrequently. The circumcentre (x_σ, y_σ) is taken as the initial guess and a maximum of eight Newton steps are allowed. Figures 4 and 5 illustrate the results of the Newton iteration for actual data on a rather coarse grid. All velocity vectors are 1/20th of their actual length and the trajectory of a particle in the given direction over 1/10 s is indicated by broken lines. Even in the cyclic case the approximation to $(x(t_m), y(t_m))$ is adequate considering the relative size of the velocity vector $\mathbf{q}$.

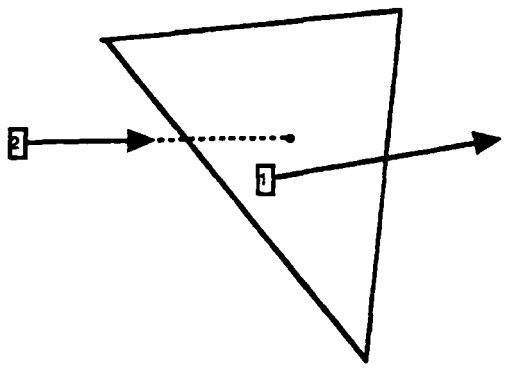

Figure 4. Newton iterates for energy equation; converged

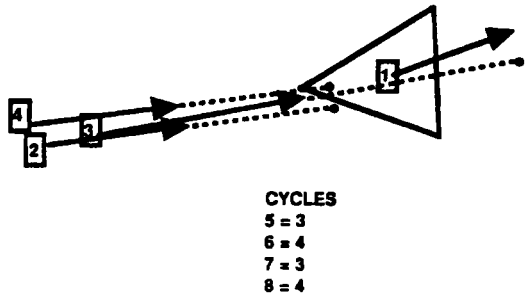

Figure 5. Newton iterates for energy equation: cyclic

The temperatures found in (17) are approximations at the circumcentres of the triangles. However, the temperature at an arbitrary point in the domain is needed, for example, when plotting isotherms or when evaluating $T(x(t_m), y(t_m), t_m)$ in (14). We use constant or linear interpolation within each triangle for this purpose. Unless stated otherwise, linear interpolation is used and this requires approximating the temperatures at the vertices of the triangulation. The temperature for an interior vertex I is determined by the formula

$$T_{\mathrm{I}} = \sum_{i=1}^{k} \left(d_i^{-1} \Big/ \sum_{j=1}^{k} d_j^{-1} \right) T_i, \tag{18}$$

where T_i is the temperature at the circumcentre of the ith triangle sharing vertex I and d_i is the distance from this circumcentre to vertex I; see Figure 6. Along the boundary, the vertex temperatures are determined by interpolation to boundary data.

Finally, we note that a Newton approximation of the point $(x(t_m), y(t_m))$ may fall outside the flow domain. In such a case the time step is adjusted so that the iterate falls on a boundary segment. To be more specific, with reference to Figure 7, suppose that $\mathbf{R}_1$ is the approximation to $(x(t_m), y(t_m))$ that is outside Ω. Then $\mathbf{R}_2 = (x^*, y^*)$ on $\partial\Omega$ and time t^* are determined by

$$\mathbf{R}_2 = \mathbf{V}_2 + \beta(\mathbf{V}_1 - \mathbf{V}_2) = \mathbf{P}_\sigma - \alpha \mathbf{q}_\sigma, \tag{19}$$

$$t^* = \begin{cases} t_{m+1} - (x_\sigma - x^*)/q_1 & \text{if} \quad q_1 \neq 0, \\ t_{m+1} - (y_\sigma - y^*)/q_2 & \text{if} \quad q_2 \neq 0. \end{cases} \tag{20}$$

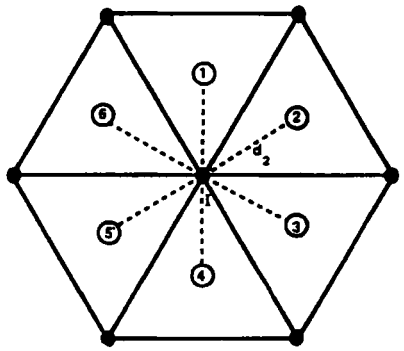

Figure 6. Temperature at interior vertex

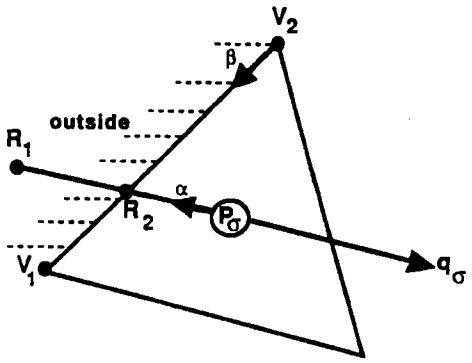

Figure 7. Particle path outside Ω

Note that (19) reduces to two linear equations in the two unknown parameters α and β. The approximation to the total derivative in (11) is then replaced by

$$\frac{dT_\sigma}{dt} \approx \frac{T(x_\sigma, y_\sigma, t_{m+1}) - T(x^*, y^*, t^*)}{t_{m+1} - t^*}.$$

3. COVOLUME DISCRETIZATION OF NAVIER–STOKES EQUATIONS

Referring again to Figure 2, the semidiscrete form of the continuity equation (1) is obtained by integrating (1) over each triangle, using the divergence theorem and making the following approximations:

$$\int_\sigma \frac{\partial \rho}{\partial t}\, dA \approx A_\sigma \frac{d\rho_\sigma}{dt}, \tag{21}$$

$$\int_\sigma \nabla \cdot (\rho \mathbf{q})\, dA = \int_{\partial\sigma} \rho \mathbf{q} \cdot N\, ds \approx \sum_{I=\mathrm{P,Q,S}} (N \cdot \mathbf{n}_I)[(\rho \mathbf{q})_I \cdot \mathbf{n}_I] h_I. \tag{22}$$

Combining these discrete continuity equations for each of the N_T triangles, we obtain the linear system

$$AD_1 \boldsymbol{\phi} = \mathbf{s}, \tag{23}$$

where $\phi_j \equiv (\rho \mathbf{q})_j \cdot \mathbf{n}_j$ is the mass velocity normal to the jth triangle side, the $N_S \times N_S$ matrix $D_1 = \mathrm{diag}(h_j)$, where N_S is the number of triangle sides in the grid, and the $N_T \times N_S$ matrix A is given by

$$a_{i,j} = \begin{cases} 1 & \text{if } \mathbf{n}_j \text{ is an outward normal on side } j \text{ of triangle } i, \\ -1 & \text{if } \mathbf{n}_j \text{ is an inward normal on side } j \text{ of triangle } i, \\ 0 & \text{if } \mathbf{n}_j \text{ is not associated with triangle } i. \end{cases}$$

The $N_T \times 1$ vector $\mathbf{s}$ contains boundary data and an approximation of $-A_i\, d\rho_i/dt$ corresponding to triangle i. Since the energy equation has been decoupled and solved at time t_{m+1}, new time densities are known from (4) and $d\rho/dt$ is approximated using a backward difference approximation.

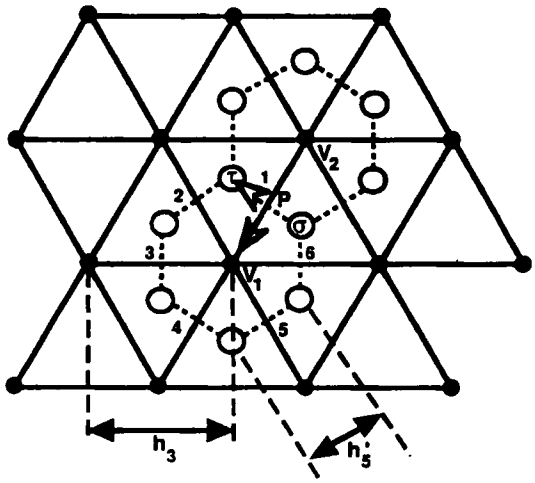

Figure 8. Discretization of momentum equation

We discretize the vector momentum equation (2) at midside P by first projecting it into $\mathbf{n}_P$. This is the same approach as was taken in References 2–5 and 8–10. We observe that

$$-\mu\Delta\mathbf{q}\cdot\mathbf{n}_P=\mu\left(\frac{\partial\omega}{\partial\mathbf{s}_P}-\frac{\partial(\nabla\cdot\mathbf{q})}{\partial\mathbf{n}_P}\right), \tag{24}$$

where $\omega\equiv-\partial q_1/\partial y+\partial q_2/\partial x$ is the *scalar vorticity*. Also, the pressure gradient term

$$\nabla p\cdot\mathbf{n}_P=\frac{\partial p}{\partial\mathbf{n}_P}, \tag{25}$$

where $\partial/\partial\mathbf{n}_P$ and $\partial/\partial\mathbf{s}_P$ denote the directional derivatives in the directions $\mathbf{n}_P$ and $\mathbf{s}_P$. Furthermore, with regard to the convection term we have

$$\begin{aligned}\nabla\cdot(\rho\mathbf{q}\mathbf{q}^T)\cdot\mathbf{n}_P&=\nabla\cdot[(\rho\mathbf{q})\mathbf{q}\cdot\mathbf{n}_P]\\&=(\mathbf{q}\cdot\mathbf{n}_P)\nabla\cdot(\rho\mathbf{q})+\rho\mathbf{q}\cdot\nabla(\mathbf{q}\cdot\mathbf{n}_P)\\&=-\frac{\partial\rho}{\partial t}(\mathbf{q}\cdot\mathbf{n}_P)+\rho|\mathbf{q}|\frac{\partial}{\partial\mathbf{q}}(\mathbf{q}\cdot\mathbf{n}_P),\end{aligned}$$

where $\partial/\partial\mathbf{q}$ denotes differentiation in the direction of $\mathbf{q}$.

It follows that the projected momentum equation can be written as

$$\frac{\partial(\rho\mathbf{q}\cdot\mathbf{n}_P)}{\partial t}+\mu\left(\frac{\partial\omega}{\partial\mathbf{s}_P}-\frac{\partial(\nabla\cdot\mathbf{q})}{\partial\mathbf{n}_P}\right)-\frac{\partial\rho}{\partial t}(\mathbf{q}\cdot\mathbf{n}_P)+|\rho\mathbf{q}|\frac{\partial}{\partial\mathbf{q}}(\mathbf{q}\cdot\mathbf{n}_P)=-\frac{\partial p}{\partial\mathbf{n}_P}+\mathbf{f}\cdot\mathbf{n}_P, \tag{26}$$

where ρ, $\mathbf{q}$ and $\mathbf{f}$ are evaluated at P.

Referring to Figure 8, we approximate the pressure gradient term in (26) by

$$\frac{\partial p}{\partial\mathbf{n}_P}\approx\frac{P_\tau-P_\sigma}{h_P'}. \tag{27}$$

The viscous term (24) is discretized using approximations to the scalar vorticity at vertices of triangles and the divergence at circumcentres of triangles. At the midside node P

$$\mu\left(\frac{\partial\omega}{\partial \mathbf{s}_P}-\frac{\partial(\nabla\cdot\mathbf{q})}{\partial \mathbf{n}_P}\right)\Bigg|_P \approx \mu\left(\frac{\omega_{V_1}-\omega_{V_2}}{h_P}-\frac{(\nabla\cdot\mathbf{q})_\tau-(\nabla\cdot\mathbf{q})_\sigma}{h'_P}\right), \tag{28}$$

where the scalar vorticity at V_i is area averaged over the Voronoi polygon Ω_{V_i} containing V_i.[4,5,8–10] For example, recall that $\int_{\Omega_{V_1}}\omega\,d\mathbf{a}=\int_{\partial\Omega_{V_1}}\mathbf{q}\cdot\mathbf{T}\,ds$, where the vector $\mathbf{T}$ is a unit tangent vector to $\partial\Omega_{V_1}$ directed in the counterclockwise sense along $\partial\Omega_{V_1}$. Note that since $\mathbf{T}=(\mathbf{T}\cdot\mathbf{n}_i)\mathbf{n}_i$ on side i, it is reasonable to approximate ω_{V_1} by

$$\omega_{V_1}\approx\left(\sum_{i=1}^{6}(\mathbf{q}\cdot\mathbf{n}_i)(\mathbf{T}\cdot\mathbf{n}_i)h'_i\right)\Big/\text{area}(\Omega_{V_1}). \tag{29}$$

The divergence $(\nabla\cdot\mathbf{q})_\sigma$ is also approximated by area averaging, i.e. the right side of (22) is divided by A_σ and $(\rho\mathbf{q})_I$ is replaced by $\mathbf{q}_I$.

It should be remarked that for thermally expandable flows we have chosen normal components of mass velocities, $\phi_P\equiv(\rho\mathbf{q})_P\cdot\mathbf{n}_P$, at midside nodes as the primitive variables. Thus in (29) the normal velocity components are computed as

$$\mathbf{q}\cdot\mathbf{n}_P=\phi_P/\rho_P, \tag{30}$$

where ρ_P is the density at the midside node P and is determined by linear interpolation of the circumcentre densities ρ_σ and ρ_τ of the two triangles sharing side P.

So far the discretizations are the same as presented in References 4, 5, 9 and 10. However, we now consider a different approach to handling the convective term in (26). Since (26) is a *scalar* momentum equation, we proceed in a manner similar to Section 2 for the energy equation. Let $\mathbf{r}_P=(x(t),y(t))$ be the path followed by a fluid particle that is at mesh point $P=(x_P,y_P)$ at time t_{m+1} (Figure 9). Then $d\mathbf{r}_P/dt=(\dot{x},\dot{y})=\mathbf{q}$ is the velocity of the particle along the path $\mathbf{r}_P$. Further, with $u\equiv\mathbf{q}\cdot\mathbf{n}_P$, a scalar function of x, y and t, we have along the path $\mathbf{r}_P$

$$\frac{du}{dt}=\nabla u\cdot\mathbf{q}+\frac{\partial u}{\partial t}. \tag{31}$$

Hence, recalling that $\partial\rho/\partial t=-\nabla\cdot(\rho\mathbf{q})$, we have from (31) that the projected momentum equation (26) can be rewritten as

$$\rho\frac{du}{dt}+\mu\left(\frac{\partial\omega}{\partial \mathbf{s}_P}-\frac{\partial(\nabla\cdot\mathbf{q})}{\partial \mathbf{n}_P}\right)=-\frac{\partial p}{\partial \mathbf{n}_P}+\mathbf{f}\cdot\mathbf{n}_P \tag{32}$$

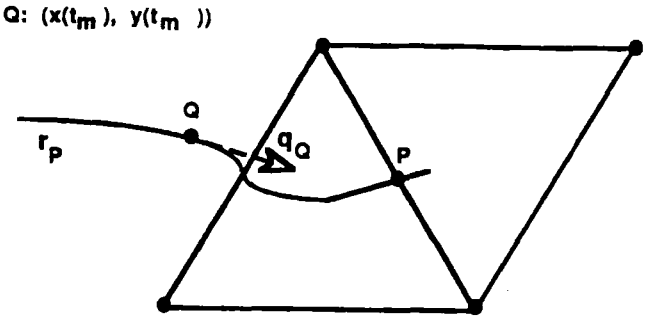

Figure 9. Particle curve through midside mesh point (x_P, y_P)

along the path $\mathbf{r}_P$. That is, the non-viscous terms on the left side of (26) are replaced by the single temporal term $\rho\, du/dt$. The other terms in (32) have been discretized at time t_{m+1} and $\rho\, du/dt$ is approximated by a backward difference, i.e.

$$\left(\rho \frac{du}{dt}\right)_P^{m+1} \approx \rho_P^{m+1} \frac{u_P^{m+1} - u(x(t_m), y(t_m), t_m)}{\Delta t_m}. \tag{33}$$

Here $u(x(t_m), y(t_m), t_m) = \mathbf{q}(x(t_m), y(t_m), t_m) \cdot \mathbf{n}_P$ is the component of velocity in the direction $\mathbf{n}_P$ at a point $(x(t_m), y(t_m))$ on the curve $\mathbf{r}_P$ through midside point $P = (x_P, y_P)$. In the time interval $[t_m, t_{m+1}]$ a particle of fluid follows $\mathbf{r}_P$ from the point $(x(t_m), y(t_m))$ to (x_P, y_P).

The problem now reduces to finding this point $(x(t_m), y(t_m))$ on the curve $\mathbf{r}_P$ The procedure is identical with that described in Section 2 for the curve $\mathbf{r}_\sigma$ except that the circumcentre σ is replaced by a midside point P. We solve a *non-linear* system

$$\begin{aligned} x(t_m) + \Delta t_m q_1(x(t_m), y(t_m), t_m) &= x_P, \\ y(t_m) + \Delta t_m q_2(x(t_m), y(t_m), t_m) &= y_P, \end{aligned} \tag{34}$$

e.g. by using Newton's method. This allows us to evaluate $u(x(t_m), y(t_m), t_m)$ in (33).

Combining (33), (27) and (28), we obtain our covolume approximation to (32) at mesh point P. Considering each such midside of the triangulation, the discrete momentum equation obtained is of the form

$$Q\phi = D_2^{-1} A^T \mathbf{p} + \mathbf{b}, \tag{35}$$

where the $N_S \times N_S$ matrix Q contains the couplings associated with the viscous and temporal terms, $\mathbf{b} \in \mathbb{R}^{N_S}$ is the vector of body forces and/or boundary data and $\mathbf{p} \in \mathbb{R}^{N_T}$ is the vector of pressures associated with triangle circumcentres. The $N_S \times N_T$ diagonal matrix D_2 has h'_P for the row associated with midside P (cf. (27)). Unlike other methods, the discrete momentum equation is *linear*; the non-linearity has been shifted to the individual systems (34) resulting from integrating backwards along the particle curves.

If we multiply (35) by D_2 and define $\mathbf{U} \equiv D_1 \phi$, then (23) and (35) combine to give the $N_S + N_T$ system

$$\begin{bmatrix} D_2 Q D_1^{-1} & A^T \\ A & 0 \end{bmatrix} \begin{bmatrix} \mathbf{U} \\ \mathbf{p} \end{bmatrix} = \begin{bmatrix} D_2 \mathbf{b} \\ \mathbf{s} \end{bmatrix} \tag{36}$$

to be solved at each time step.

The velocity vector $\mathbf{q}$ is approximated at the ith triangle midside as $\mathbf{q}_i = u_i \mathbf{n}_i + v_i \mathbf{s}_i$, where the normal component u_i is a primitive variable in the covolume method. However, v_i must be reconstructed using only boundary data and the normal flows u_i. Two schemes have been presented[4,6] which will reproduce *constant* flow fields, but neither will reproduce *linear* flow fields. In Reference 9 we presented two methods that reproduce constant and linear flow fields. For completeness we describe one of these methods here, though either is appropriate. Assume that the velocity $\mathbf{q}$ is linear and of the form

$$\mathbf{q} = A \begin{pmatrix} 1 \\ x \\ y \end{pmatrix}, \tag{37}$$

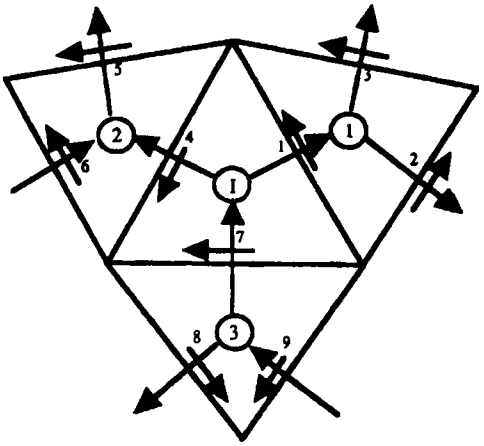

Figure 10. A triangle and three neighbours

where the 2×3 matrix $A = [\mathbf{a}_1 \ \mathbf{a}_2 \ \mathbf{a}_3] = [a_{ij}]$. Referring to Figure 10, we note that the velocity components for a given triangle I and its three neighbouring triangles are labelled 1–9. We define the 2×3 matrix Q_1 and the 3×3 matrix X_1 by

$$Q_1 = [\mathbf{q}_1 \ \mathbf{q}_2 \ \mathbf{q}_3], \qquad X_1 = \begin{bmatrix} 1 & 1 & 1 \\ x_1 & x_2 & x_3 \\ y_1 & y_2 & y_3 \end{bmatrix},$$

where $\mathbf{q}_i$ is the velocity vector at point i. Similarly, we define Q_2, Q_3, X_2 and X_3. Since the triangles have positive area, it follows that X_i^{-1} exists and from (37) we have

$$A = Q_1 X_1^{-1} = Q_2 X_2^{-1} = Q_3 X_3^{-1} \tag{38}$$

or

$$A = \frac{1}{3} \sum_{i=1}^{3} Q_i X_i^{-1}. \tag{39}$$

Using (38) and (39), we obtain e.g.

$$Q_1 = \frac{1}{3} \left(\sum_{i=1}^{3} Q_i X_i^{-1} \right) X_1, \tag{40}$$

from which it follows that

$$v_j = \mathbf{q}_j \cdot \mathbf{s}_j = \frac{1}{3} \left(v_j + \sum_{k=4}^{6} [X_2^{-1} X_1]_{j,k-3} v_k (\mathbf{s}_k \cdot \mathbf{s}_j) + \sum_{k=7}^{9} [X_3^{-1} X_1]_{j,k-6} v_k (\mathbf{s}_k \cdot \mathbf{s}_j) \right), \quad j = 1, 2, 3. \tag{41}$$

In (41) we have made use of the notation $[X]_{ij}$ to denote the element in row i and column j of matrix X. Repeating (40) and (41) for triangles 2 and 3, we obtain nine equations in nine unknowns. However, it can be shown that this system is singular. Thus we add to the system two equations which state that $\mathbf{q}$ at

the centroid C of triangle I belongs to the same linear flow field. This can be expressed in terms of triangle 1 as (for example)

$$\mathbf{q}_C = A\begin{pmatrix} 1 \\ x_C \\ y_C \end{pmatrix} = Q_1^{-1}X_1\begin{pmatrix} 1 \\ x_C \\ y_C \end{pmatrix}. \tag{42}$$

However, the point C has barycentric co-ordinates $(\frac{1}{3}, \frac{1}{3}, \frac{1}{3})$ and $\mathbf{q}$ being linear implies

$$\mathbf{q}_C = \tfrac{1}{3}(\mathbf{q}_1 + \mathbf{q}_4 + \mathbf{q}_7). \tag{43}$$

Substituting (43) into (42) yields two scalar equations in the unknowns v_1, v_2, v_3, v_4 and v_7. These two equations combined with the earlier nine equations produce an 11×9 system which we have found in all our computations to have full rank. We use the LINPACK subroutine SQRSL to obtain the unique least squares solution of this system.

If one of the triangles, say triangle 2, does not exist and link 4 crosses the boundary of the flow region Ω, then v_4 is assumed given as boundary data. The variables v_5 and v_6 are non-existent and the system to be solved is now 8×6.

In general the above procedure is repeated twice for each link, since there are two triangles sharing each interior link of the grid. This generates two approximations for the tangential flow on such a link which are then averaged.

Next we present a variable reduction technique which replaces the $N_T + N_S$ system (36) by an equivalent system of dimension $N_S - N_T$. This network method (the *dual variable method*) was presented in References 2–5, 9 and 10 and is an extension of earlier work[12,13,21–29,33] to triangular grids.

In network terminology[30] the sides (links) and vertices (nodes) of the Voronoi polygons form a directed network Γ, while those of the triangles constitute its dual Γ^*. Each link of Γ carries a *flow* that is an approximation of the normal mass flux rate across a triangle's side, while each node of Γ carries a *state* that is an approximation of the pressure at the circumcentre of a triangle. The matrix A in (23) is the *incidence matrix* of the network Γ, equations (23) are its *node laws* and equations (35) constitute the *link characteristics*.

Once the above identifications have been made, the dual variable method is applicable. The dual variables are states on the nodes of Γ^*, i.e. the vertices of the triangles. If the flow region is simply connected, then the boundaries of the Voronoi polygons form a basis of elementary cycles for Γ and an *exact* representation of the most general flows satisfying the node laws can be given in terms of the dual variables. Moreover, a transformation of the link characteristics then produces a closed system that determines the dual variables.

The specific application of these ideas to (36) proceeds as follows. The dimension of the elementary cycle basis is known to be $N_S - N_T$ and each cycle gives a simple prescription for the determination of a linearly independent vector in $\ker A$. Thus $\dim(\ker A) = N_S - N_T$ and, using the elementary cycles of Γ, it is straightforward[4] to construct an $N_S \times (N_S - N_T)$ fundamental matrix C whose columns form a basis for $\ker A$. If $U = D_1\phi$ and $U_0 = D_1\phi_0$, where ϕ_0 is any particular solution of (23), then $U - U_0 \in \ker A$. Hence $U - U_0 = C\boldsymbol{\gamma}$ for some vector of dual variables, $\boldsymbol{\gamma} = (\gamma_1, \cdots, \gamma_{N_S - N_T})^T$, and so

$$\phi = D_1^{-1}(C\boldsymbol{\gamma} + \mathbf{U}_0). \tag{44}$$

Equation (44) expresses the N_S unknown mass flux rates ϕ_j in terms of $N_S - N_T$ dual variables. If we substitute (44) into (36) and recall that $U = D_1\phi$, then the second block row is trivially satisfied and the first block row becomes

$$D_2QD_1^{-1}C\boldsymbol{\gamma} + A^T\mathbf{p} = D_2\mathbf{b} - D_2QD_1^{-1}\mathbf{U}_0.$$

Multiplication by C^T eliminates the pressures (since $AC = 0$), resulting in a system of dimension $N_S - N_T$, the *dual variable system*

$$C^T(D_2QD_1^{-1})C\boldsymbol{\gamma} = C^T(D_2\mathbf{b} - D_2QD_1^{-1}\mathbf{U}_0). \tag{45}$$

This is solved at each time step, the velocities are recovered from (44) and (if desired) the pressures are computed from the triangular system $A^T\mathbf{p} = \mathbf{c}$ obtained from (36).

Based on the estimates given in Reference 31, for a fine grid $N_T \approx \frac{2}{3}N_S$. Hence the primitive system is of dimension $N_S + N_T \approx \frac{5}{3}N_S$, while the dual variable system is of dimension $N_S - N_T \approx \frac{1}{3}N_S$. *We conclude that the dual variable system is a factor of five smaller than the primitive system.* See References 4 and 5 for more details on the dual variable method for triangular grids.

The normal velocity components u_i that are determined by the covolume method and the tangential velocity components v_i that are subsequently determined by a reconstruction procedure such as the one outlined above provide approximations $\mathbf{q}_i = u_i\mathbf{n}_i + v_i\mathbf{s}_i$ for the velocity at the midpoints of each of the triangle sides in the grid. However, the velocity $\mathbf{q}$ at an arbitrary point within the flow domain is needed, for example, when plotting the vector field or when evaluating $\mathbf{q}(x(t_m), y(t_m), t_m)$ in (16) or (31). We use linear interpolation within each triangle of the mesh. This requires approximating the velocity $\mathbf{q}$ at the vertices of the triangulation.

Consider the triangle vertex I in Figure 11 and the associated Voronoi polygon. For each point A_i we have a velocity $\mathbf{q}_i$. We choose three of these points, e.g. A_1, A_3 and A_5, such that the triangle $A_1A_3A_5$ contains vertex I and we define

$$\mathbf{q}_I \equiv \alpha_1\mathbf{q}_1 + \alpha_3\mathbf{q}_3 + \alpha_5\mathbf{q}_5,$$

where $\{\alpha_1, \alpha_3, \alpha_5\}$ are the barycentric co-ordinates of point I in the triangle $A_1A_3A_5$. Note that the determination of the triple of indices $\{1, 3, 5\}$ and the barycentric co-ordinates of vertex I is a one-time computation done as a preprocessor step outside the time loop.

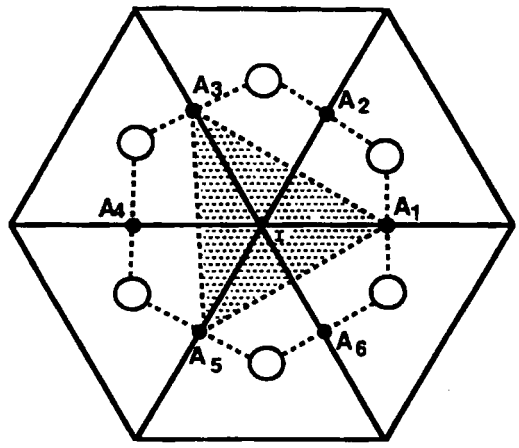

Figure 11. Interpolation of vertex velocities

4. NUMERICAL EXAMPLES

4.1. *Rotating exponential form*

Consider a square domain $(-1, 1) \times (-1, 1)$ in which an incompressible fluid is rotating with velocity $\mathbf{q} = (y, -x)$ around the origin. There is no heat source: $Q = 0{\cdot}0$. The conductivity $k = 0{\cdot}0$, the density $\rho = 1{\cdot}0$ and the specific heat $c_p = 1{\cdot}0$. The initial temperature is

$$T(x, y, 0) = \begin{cases} e^{-5\times10^{-4}/(|\mathbf{x}-\mathbf{x}_0|^2-0{\cdot}25^2)^2} e^{0{\cdot}128}, & |\mathbf{x} - \mathbf{x}_0| < 0{\cdot}25, \\ 0, & \text{otherwise}, \end{cases}$$

where $\mathbf{x}_0 = (0{\cdot}5, 0{\cdot}0)$. Equations (1) and (2) are not needed, since the velocity field is assumed known. The initial temperature distribution is thus rotated about the origin as time advances. For this example the trapezoidal rule approximation to the integral in (15) was used.

Figure 12 illustrates the Delaunay tessellation used, which contains $N_T = 1942$ triangles. The time step $\Delta T = \pi/6$ and piecewise constant interpolation was used in (14). Figure 13 illustrates the form at $t = 0$, $\pi/2$, π and $3\pi/2$.

4.2. *Natural convection in a square cavity*

This is a typical benchmark problem involving thermally driven flows.[17,32] Consider a square cavity of side D. The top and bottom are insulated, while the two sides are differentially heated, with T_h on the left and T_c on the right. The walls of the cavity are assumed to be no-slip (i.e. the tangential and normal components of the velocity vanish on the walls). The solution to this problem depends on the value of the *Rayleigh number*

$$Ra = \frac{\beta g(T_h - T_c)D^3}{\mu\alpha/\rho},$$

where $\beta = (-1/\rho)(\partial\rho/\partial T)$ is the coefficient of volumetric expansion, g is the gravitational constant and $\alpha \equiv k/\rho c_p$ is the thermal diffusivity. It is well known that the problem becomes increasingly more difficult to solve numerically as the Rayleigh number increases. The body force term in (2) was taken to be $\mathbf{f} = (0, \rho g)^T$, where g is the gravitational constant.

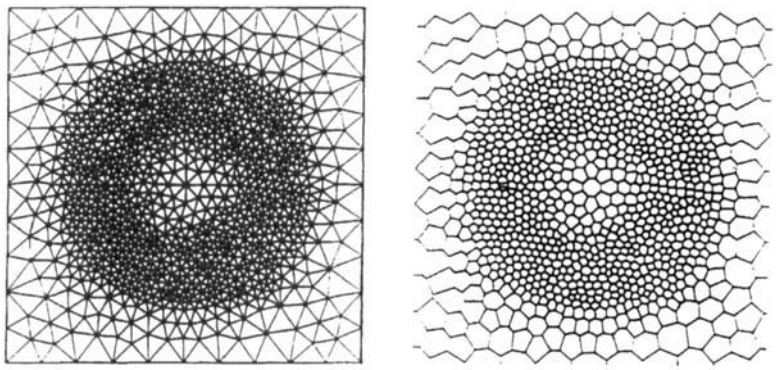

Figure 12. Delaunay and Voronoi tessellations for rotating exponential form

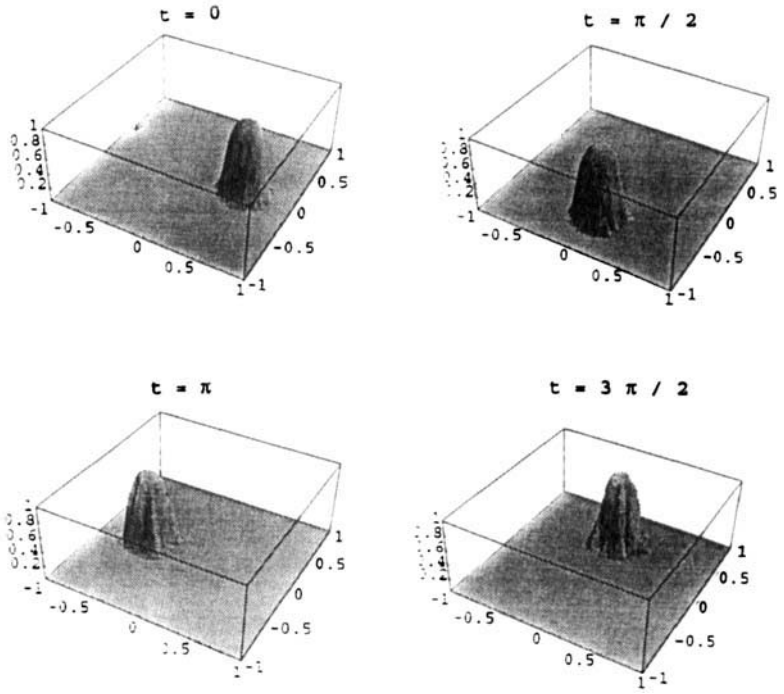

Figure 13. Rotating exponential form for $t=0$, $\pi/2$, π and $3\pi/2$

The triangulation in Figure 14 was used with $D=0{\cdot}08717$ ft. The values of the parameters in (1)–(4) were chosen* corresponding to air and the temperature drop was chosen so that $Ra=10^4$. The grid contains $N_T=730$ triangles and $N_S=1059$ (interior) triangle sides. The fluid dynamics problem involves a primitive system with 1789 unknowns, while the dual variable system has 329 unknowns. Note that $N_S+N_T=1789$ and $N_S-N_T=329$.

Figure 15 presents the isotherms at steady state. These results correspond to 600 steps of the CL method with a time step of 0·01 s. Equation (16) was used, as was linear interpolation within triangles.

The heat transfer at the hot wall is defined by the local Nusselt number

$$Nu=-\frac{L}{T_m}\frac{\partial T}{\partial x},$$

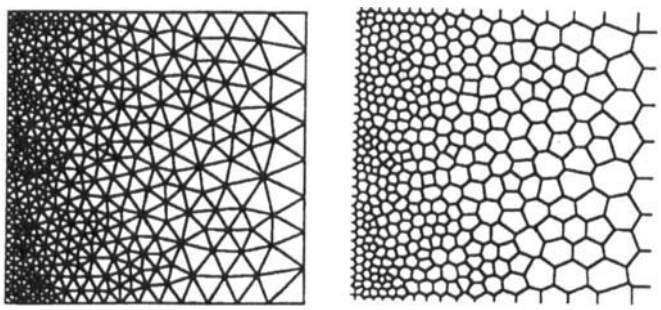

Figure 14. Tessellations for natural convection in a square cavity

* $\rho=0{\cdot}08634$ lb ft^{-3}, $g=32{\cdot}1739$ ft s^{-2}, $\beta=0{\cdot}218\times10^{-2}$ °F^{-1}, $\mu=1{\cdot}5664\times10^{-5}$ lb s^{-1} ft^{-1}, $c_P=0{\cdot}243$ BTU lb^{-1} °F^{-1}, $k=5{\cdot}3610\times10^{-6}$ BTU ft^{-1} s^{-1} °F^{-1}, $T_h=10{\cdot}0$ °F and $T_c=0{\cdot}0$ °F.

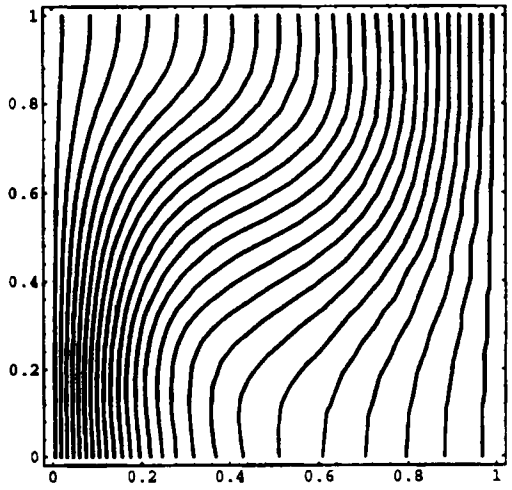

Figure 15. Isotherms for natural convection, $Ra = 10^4$

where the reference length $L = D$ and the reference temperature $T_m = (T_h - T_c)/2$. The local mesh refinement along the hot wall in Figure 14 is to facilitate the calculation of Nu. For this problem we found that the maximum and minimum values of Nu are 3·55 and 0·59. These compare well, for example, with the values of 3·51 and 0·59 determined by de Vahl Davies and Leong in Reference 32.

4.3. Flow around a heated rod

To illustrate the use of the CL method in the simulation of homogeneous two-phase flow, we consider a heated rod of radius 0·1 ft centred one-third of the distance down a 1 ft by 1·5 ft channel; see also Reference 29. Figure 1 contains the Delaunay tessellation on which the semidiscretizations were made. For this problem $N_T = 586$ and $N_S = 861$. Hence the size of the primitive system is 1447, while that of the dual variable system is 275. The problem utilizes the generalized forms (3a) and (4a) of the energy and state equations.

The transient was initiated from a steady state in which slightly subcooled water (system pressure $p^* = 1000$ lbf in^{-2} and enthalpy $H = 535$ BTU lb^{-1}) enters the channel on the left with horizontal mass velocity $\rho q_1(0, y) = 12{\cdot}5$ lb ft^{-2} s^{-1}. The downstream boundary condition is $p(1{\cdot}5, y) =$ 1000 lbf in^{-2} and a freestream condition is simulated at $y = 0$ and 1·0: $\rho q_1(x, 0) = \rho q_1(x, 1{\cdot}0) = 12{\cdot}5$ lb ft^{-2} s^{-1} and $\rho q_2(x, 0) = \rho q_2(x, 1{\cdot}0) = 0{\cdot}0$. Heat is added to the 24 cells surrounding the rod at a rate $Q = 1050$ BTU ft^{-3} s^{-1}.

The quality χ of the mixture is defined by

$$\chi = \frac{H - H_f(p^*)}{H_g(p^*) - H_f(p^*)},$$

where $H_f(p^*)$ and $H_g(p^*)$ are the enthalpies of saturated liquid and vapour respectively. Thus in our example $\chi = 0{\cdot}0$ corresponds to no steam while $\chi = 1{\cdot}0$ corresponds to a 'mixture' of 100 per cent steam.

The CL method (equation (16)) was used to numerically solve this problem. A time step of 0·125 s was used for 320 steps. Figures 16 and 17 show respectively some of the instantaneous quality contours and streamlines 40 s into the transient. At this time the maximum quality is 15·3 per cent. This high-quality mixture is in the region immediately behind the rod.

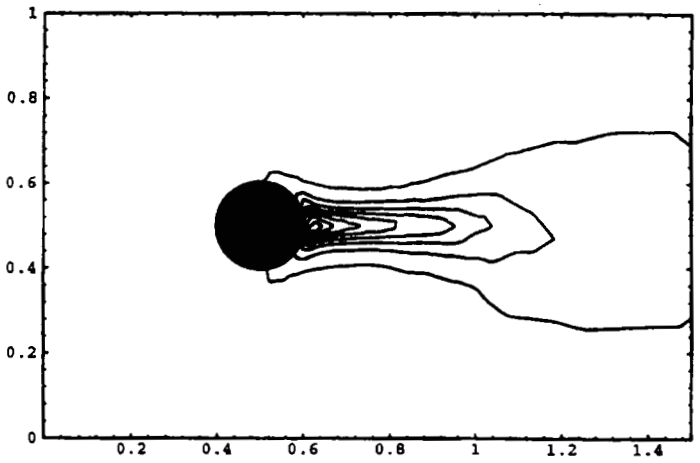

Figure 16. Quality contours at 40 s

Note that although the flow region contains a two-phase mixture at $t = 40$, the contours of Figure 17 resemble those of laminar flow. This suggests that for the current choice of time step and grid the CL method is overly dissipative. Indeed, a von Neumann analysis of the model problem considered in the Appendix reveals that up to a factor of unit modulus the CL method amplification factors are identical in form with those of the explicit upwind method. (The interpolation weight α in the CL method plays the role of the Courant number c in the explicit upwind method.) In view of this, the graphical results of Figure 17 should come as no surprise.

As we have already noted, for a given spatial mesh the treatment of convection effects by the CL method is more accurate for *larger* time steps. Thus it appears advantageous to use a time step significantly greater than 0·125 in this example. Unfortunately, the presence of an impervious boundary (the surface of the rod) prevents this. To see why, recall that the basic idea of the CL method is to numerically integrate a total derivative representing the temporal and convection terms along an approximate particle path that terminates at a given grid point. Clearly, it is physically meaningless for this path to emanate from or pass through a solid. However, this is precisely what occurs in triangles immediately downstream of the rod unless the time step is sufficiently small, i.e. of the order of 0·125.

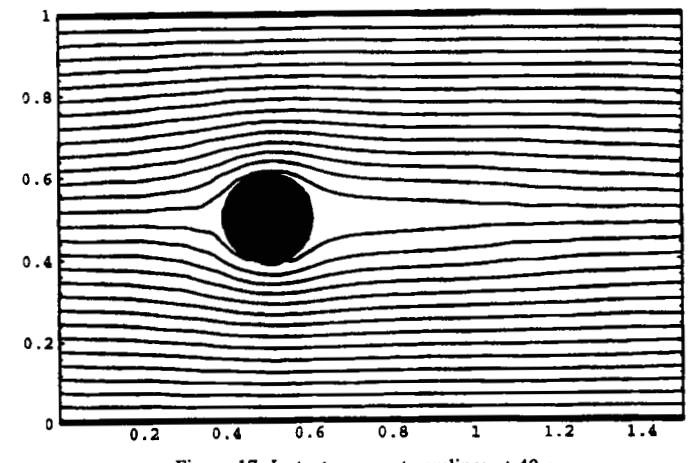

Figure 17. Instantaneous streamlines at 40 s

Presumably, the accuracy of the numerical solution would improve by refining the spatial grid and, if necessary, adjusting the time step.

5. CONCLUSIONS

The numerical solution of thermally expandable flows on triangular grids using a characteristic-like method was investigated. An approximate particle trajectory was determined and the temporal and convective terms were combined and integrated backwards in time along the trajectory to produce finite difference approximations.

Delaunay and Voronoi tessellations were used to generate dual grids that decompose the flow region into covolumes. The advantages of such decompositions are the ability to generate a grid for virtually arbitrary flow regions without resorting to costly mapping techniques, the ability to grade the grid to achieve local refinement and the availability of highly developed automatic mesh generators.

The covolume discrete primitive system can be interpreted as node laws and link characteristics of a directed network defined by the Voronoi polygons associated with a triangular grid. The dual variable method was used to obtain an equivalent system that is less than one-fifth the size of the primitive system. In addition, this dual variable approach, unlike e.g. penalty methods, guarantees that mass is conserved identically.

Numerical results were presented illustrating the flexibility of this approach.

ACKNOWLEDGEMENT

This research was supported by the Electric Power Research Institute under Grant RP: 8006-24.

APPENDIX: CONVERGENCE ANALYSIS OF THE CL METHOD FOR THE ONE-DIMENSIONAL MODEL CONVECTION EQUATION

To obtain some idea about the accuracy of the approximate solutions produced by the CL method, we consider its application to the initial value problem

$$\partial\phi/\partial t + q\partial\phi/\partial x = 0, \quad t > 0,$$
$$\phi(x, 0) = \phi_0(x),$$

where $-\infty < x < \infty$, q is a (positive) constant and ϕ_0 is the initial data.

If $x = x(t)$ denotes the characteristic curve passing through (x, t) and satisfying $dx/dt = q$, then $\phi(x(t), t)$ satisfies $d\phi/dt = 0$. Thus, if (x_0, t_0) is any other point on the characteristic, we have $\phi(x, t) = \phi(x_0, t_0)$. In particular, if we consider a grid of points (x_j, t_m), where $x_j = jh$, $j = 0, \pm 1, \cdots$, and $t_m = m\Delta t$, $m = 0, 1, \cdots$, then

$$\phi(x_j, t_m) = \phi(x_j - \delta, t_{m-1}), \tag{46}$$

where $\delta = q\Delta t$.

For this problem the CL method at time level t_m consists of the following steps.

1. Solve

$$\frac{x_j - x_*}{\Delta t} = q \tag{47}$$

for the point $x_* = x_j - q\Delta t$.

2. Solve

$$\frac{\Phi(x_j, t_m) - \Phi(x_*, t_{m-1})}{\Delta t} = 0$$

for the approximation $\Phi(x_j, t_m)$; that is,

$$\Phi(x_j, t_m) = \Phi(x_j - \delta, t_{m-1}). \tag{48}$$

Comparing (46) and (48), we conclude that the CL method is exact at $t = t_m$ if it is exact at $t = t_{m-1}$, i.e. if $\Phi(x, t_{m-1}) = \phi(x, t_{m-1})$ for all x. However, any practical implementation of the method requires that $\Phi(x, t_{m-1})$ be reconstructed from discrete data. This is usually done by applying an interpolation scheme based on values at the grid points x_j. Therefore let us assume that $\Phi(x, t_{m-1})$ is obtained by linear interpolation of the grid point values $\Phi(x_j, t_{m-1})$. The use of linear (or other) interpolation introduces a discretization error that propagates forwards in time. To study the nature of this phenomenon, let $\phi_I(x, t)$ denote the linear interpolant of $\phi(x, t)$ and define the interpolation error $e(x, t) = \phi_I(x, t) - \phi(x, t)$. Furthermore, let $E(t) = \max_x |e(x, t)|$.

Proposition

For $m = 1, 2, \ldots$ we have

$$|\Phi(x_j, t_m) - \phi(x_j, t_m)| \leqslant \sum_{i=0}^{m-1} E(t_i), \quad j = 0, \pm 1, \ldots. \tag{49}$$

Proof. We give a proof by induction on m. By (46) we have

$$\phi(x_j, t_1) = \phi(x_j - \delta, 0),$$

while by (48)

$$\Phi(x_j, t_1) = \Phi(x_j - \delta, 0) = \phi_1(x_j - \delta, 0) = \phi(x_j - \delta, 0) + e(x_j - \delta, 0) = \phi(x_j, t_1) + e(x_j - \delta, 0).$$

Therefore

$$|\Phi(x_j, t_1) - \phi(x_j, t_1)| = |e(x_j - \delta, 0)| \leqslant E(0),$$

which verifies (49) for $m = 1$. Now assume that (49) holds for t_{m-1}, $m \geqslant 2$. Then we can write

$$\Phi(x_j, t_{m-1}) = \phi(x_j, t_{m-1}) + \varepsilon(x_j, t_{m-1}),$$

where

$$|\varepsilon(x_j, t_{m-1})| \leqslant \sum_{i=0}^{m-2} E(t_i).$$

Since $\phi(x_j, t_m) = \phi(x_j - \delta, t_{m-1})$ and, according to the linear interpolation formula,

$$\Phi(x_j, t_m) = \Phi(x_j - \delta, t_{m-1}) = \alpha\Phi(x_{k-1}, t_{m-1}) + (1 - \alpha)\Phi(x_k, t_{m-1}) \tag{50}$$

for some k and $0 \leqslant \alpha \leqslant 1$, we have

$$\begin{aligned}\Phi(x_j, t_m) &= \alpha[\phi(x_{k-1}, t_{m-1}) + \varepsilon(x_{k-1}, t_{m-1})] + (1 - \alpha)[\phi(x_k, t_{m-1}) + \varepsilon(x_k, t_{m-1})] \\ &= \alpha\phi(x_{k-1}, t_{m-1}) + (1 - \alpha)\phi(x_k, t_{m-1}) + \alpha\varepsilon(x_{k-1}, t_{m-1}) + (1 - \alpha)\varepsilon(x_k, t_{m-1}).\end{aligned}$$

Applying the definition of $\phi_1(x_j - \delta, t_{m-1})$, we get

$$\Phi(x_j, t_m) = \phi_1(x_j - \delta, t_{m-1}) + M,$$

where

$$M = \alpha\varepsilon(x_{k-1}, t_{m-1}) + (1 - \alpha)\varepsilon(x_k, t_{m-1}).$$

Hence

$$\Phi(x_j, t_m) = \phi(x_j - \delta, t_{m-1}) + e(x_j - \delta, t_{m-1}) + M = \phi(x_j, t_m) + e(x_j - \delta, t_{m-1}) + M.$$

Therefore

$$\begin{aligned} |\Phi(x_j, t_m) - \phi(x_j, t_m)| &\leqslant |e(x_j - \delta, t_{m-1})| + |M| \\ &\leqslant E(t_{m-1}) + \alpha|\varepsilon(x_{k-1}, t_{m-1})| + (1 - \alpha)|\varepsilon(x_k, t_{m-1})| \\ &\leqslant E(t_{m-1}) + \sum_{i=0}^{m-2} E(t_i) = \sum_{i=0}^{m-1} E(t_i). \end{aligned}$$

This completes the induction.

It is a simple consequence of the above argument that the CL method is, in the parlance of difference methods, 'unconditionally stable'.

Corollary 1

If $\phi_0(x)$ is bounded on $(-\infty, \infty)$, then for any choice of h and Δt we have

$$\max_j |\Phi(x_j, t_m)| \leqslant \max_j |\phi_0(x_j)|.$$

Proof. It follows from (50) that

$$|\Phi(x_j, t_m)| \leqslant \max_k |\Phi(x_k, t_{m-1})|.$$

Therefore

$$\max_j |\Phi(x_j, t_m)| \leqslant \max_k |\Phi(x_k, t_{m-1})|$$

and the result follows by repeated application of this last inequality.

As a second corollary we have the following convergence result.

Corollary 2

Let t be a fixed time level such that $t = m\Delta t$ and let the initial data ϕ_0 be twice continuously differentiable. Then there is a constant K that is independent of h and Δt such that

$$|\Phi(x_j, t) - \phi(x_j, t)| \leqslant Kt(h^2/\Delta t). \tag{51}$$

Proof. Since $\phi(x, t) = \phi_0(x - qt)$, the hypotheses imply that $\partial^2\phi/\partial x^2$ is continuous. Hence for linear interpolation we have $E(t) \leqslant Kh^2$, where K is a constant independent of h. Therefore (49) implies that

$$|\Phi(x_j, t) - \phi(x_j, t)| = |\Phi(x_j, t_m) - \phi(x_j, t_m)| \leqslant \sum_{i=0}^{m-1} E(t_i) \leqslant mKh^2 = Kt(h^2/\Delta t).$$

This establishes the corollary.

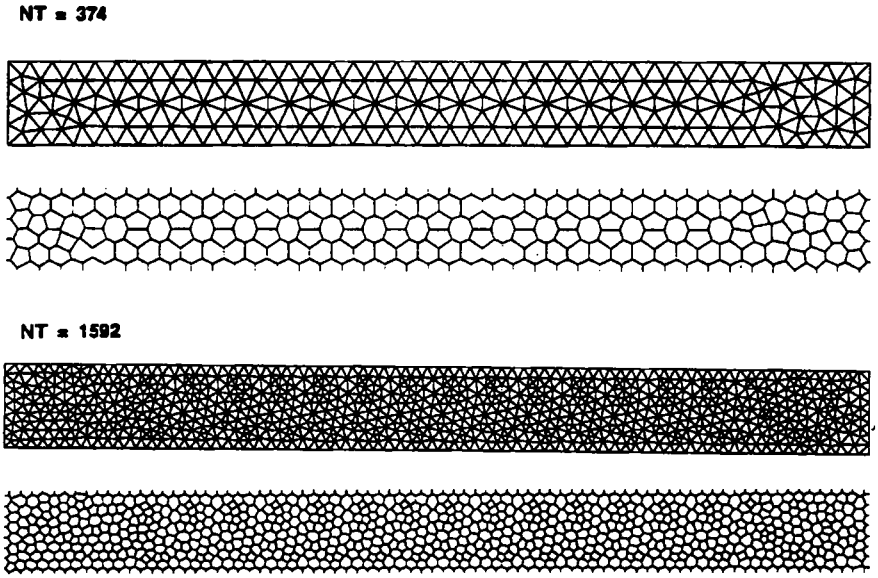

Figure 18. Delaunay and Voronoi tessellations for thermal wave

The estimate (51) shows that if the grid is refined so that the mesh ratio $\Delta t/h$ is constant, then the method is first-order in h. However, it also shows that if Δt is fixed (at any value), then we have a *second*-order method in h. This somewhat surprising result is due to the fact that for the model convection equation there is no error in the method due to time discretization—the error is introduced solely by the linear interpolation process. On the other hand, if we fix h and let Δt approach zero, the right side of (51) becomes unbounded, suggesting that in this case the accuracy of the approximate solution deteriorates. To illustrate this behaviour, we consider the following example.

Convection of thermal wave in a uniform flow field

We consider a channel $[0{\cdot}0, 10{\cdot}0] \times [0{\cdot}0, 1{\cdot}0]$ with the Delaunay and Voronoi tessellations as illustrated in Figure 18. There are $N_T = 374$ triangles in the coarse grid and $N_T = 1592$ triangles in the fine grid. The velocity field is assumed to be uniform, $\mathbf{q} = (1{\cdot}0, 0{\cdot}0)^T$, and the channel walls ($y = 0$ and 1) are taken to be adiabatic free-slip. The conductivity $k = 0{\cdot}0$, the density $\rho = 1{\cdot}0$ and the specific heat $c_p = 1{\cdot}0$. Ta ere is no heat source: $Q = 0{\cdot}0$. Initially the temperature in the channel is $T(x, y, 0) = 0{\cdot}0$ and the periodic inlet temperature is

$$T(0, y, t) = 0{\cdot}25 \cos(\pi t/3{\cdot}0).$$

Under these conditions the problem becomes one-dimensional and has as its solution the travelling wave

$$T(x, y, t) = 0{\cdot}25 \cos[\pi(x - t)/3{\cdot}0].$$

Thus the analysis given above applies. Figure 19 presents the centreline ($y = 0{\cdot}5$) temperatures at $t = 12$ s for the CL and donor cell[9] methods for various choices of time step on the coarse tessellation. For $\Delta t \geqslant 10{\cdot}0$ the CL method using (16) is exact (to within machine accuracy). However, the accuracy of the CL solution degrades as $\Delta t \to 0$ for a fixed tessellation. As mentioned above, this is due to the accumulation of interpolation errors over more and more time steps. On the other hand, in accordance with the convergence analysis, Figure 20 shows that a refinement of the spatial grid gives improved results in the CL method for the same time step $\Delta t = 0{\cdot}1$.

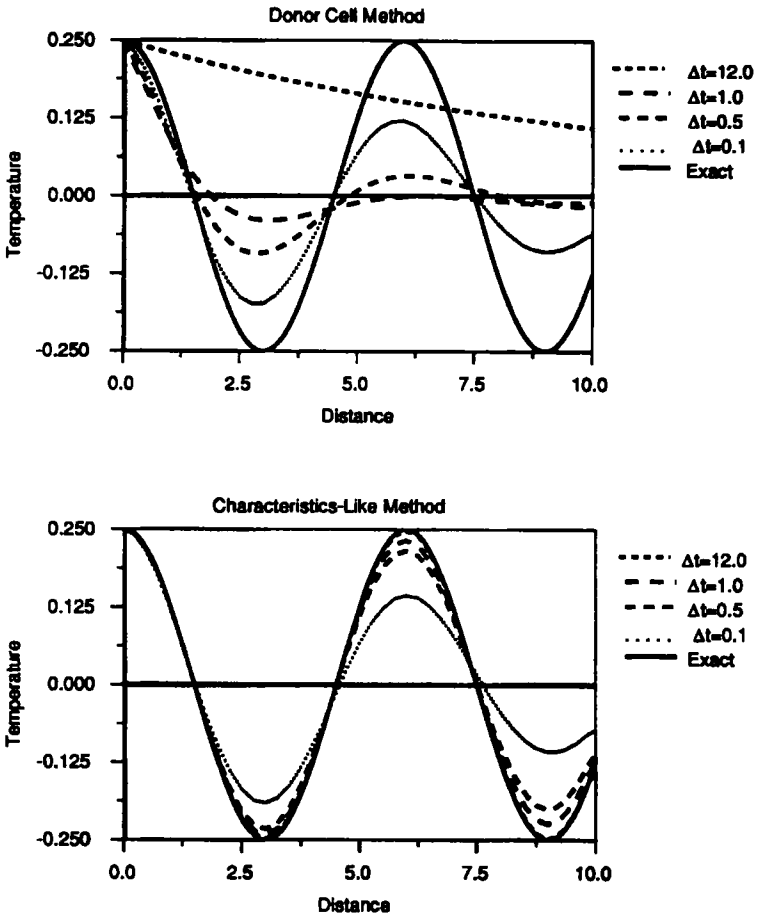

Figure 19. Centreline temperatures for coarse grid: thermal wave

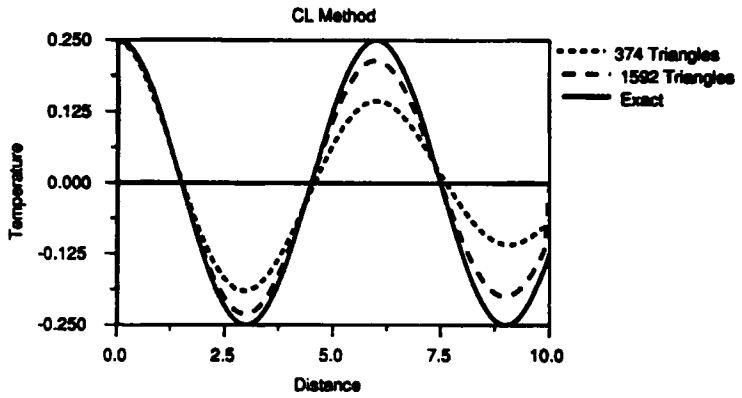

Figure 20. Centreline temperatures for $\Delta t = 0{\cdot}1$ and two tessellations

REFERENCES

1. R. H. MacNeal, 'An asymmetrical finite difference network', *Q. Appl. Math.*, **11**, 295–310 (1953).
2. J. C. Cavendish, C. A. Hall and T. A. Porsching, 'Solution of incompressible Navier–Stokes equations on unstructured grids using dual tessellations', *Int. j. numer. methods heat fluid flow*, **2**, 483–502 (1992).
3. J. C. Cavendish and C. A. Hall, 'A complementary volume approach for modelling incompressible Navier–Stokes equations on Delaunay/Voronoi tessellations', *Proc. 7th Int. Conf. on Numerical Methods in Laminar and Turbulent Flows*, Palo Alto, CA, July 1991.
4. C. A. Hall, J. C. Cavendish and W. H. Frey, 'The dual variable method for solving fluid flow difference equations on Delaunay triangulations', *Comput. Fluids*, **20**, 145–164 (1991).
5. C. A. Hall, T. A. Porsching and G. L. Mesina, 'On a network method for unsteady incompressible fluid flow on triangular grids', *Int. j. numer. methods fluids*, **15**, 1383–1406 (1992).
6. R. A. Nicolaides, 'Flow discretization by complementary volume techniques', *AIAA Paper 89-1978*, 1989.
7. R. A. Nicolaides, 'Triangular discretization for the vorticity–velocity equations', *Proc. 7th Int. Conf. on Finite Elements in Flow Problems*, Huntsville, AL, 1989, p. 1.
8. R. A. Nicolaides, 'Direct discretization of planar div–curl problems', *SIAM J. Numer. Anal.*, **29**, 32–56 (1992).
9. C. A. Hall, T. A. Porsching and P. Hu, 'Covolume–dual variable method for thermally expandable flow on unstructured triangular grids', *Int. J. Comput. Fluid Dyn.*, **2**, 111–139 (1994).
10. T. A. Porsching and C. A. Hall, 'A network method for homogeneous, thermally expandable two-phase flow on unstructured triangular grids', *Proc. Fifth Int. Topical Meet. on Nuclear Reactor Thermal Hydraulics*, Salt Lake City, UT, September 1992.
11. R. A. Nicolaides, T. A. Porsching and C. A. Hall, 'Covolume methods in computational fluid dynamics', *CFD Rev. 1995*, ed. M. Hafez and K. Oshima, pp. 279–299, John Wiley & Sons, Chichester 1995.
12. R. S. Dougall, C. A. Hall and T. A. Porsching, 'DUVAL: a computer program for the numerical solution of two-dimensional, two-phase flow problems, Vols. 1–3', *Electric Power Research Institute Rep. NP-2099*, Palo Alto, CA, 1982.
13. T. A. Porsching, 'A network model for two-fluid, two-phase flow', *Numer. Methods Partial Diff. Eqns*, **1**, 295–313 (1985).
14. W. H. Frey and J. C. Cavendish, 'Fast planar mesh generation using the Delaunay triangulation', *General Motors Research Publ. GMR-4555*, 1983.
15. D. F. Watson, 'Computing the *n*-dimensional Delaunay tessellation with applications to Voronoi polytopes', *Comput. J.*, **24**, 167–172 (1981).
16. W. H. Frey, 'Selective refinement: a new strategy for automatic node placement in graded triangular meshes', *Int. j. numer. methods eng.*, **24**, 2183–2200 (1987).
17. C. A. Hall and T. A. Porsching, *Numerical Analysis of Partial Differential Equations*, Prentice-Hall, Englewood Cliffs, NJ, 1990.
18. O. Pironneau, *The Finite Element Method for Fluids*, Wiley, New York, 1989.
19. R. Courant, E. Issacson and M. Rees, 'On the solution of nonlinear hyperbolic differential equations by finite differences', *Commun. Pure Appl. Math.*, **5**, 243 (1952).
20. J. Douglas and T. Russell, 'Numerical methods for convection-dominated diffusion problems based on combining the method of characteristics with finite difference or finite element procedures', *SIAM J. Numer. Anal.*, **5**, 871 (1982).
21. R. Amit, C. A. Hall and T. A. Porsching, 'An application of network theory to the solution of implicit Navier–Stokes difference equations', *J. Comput. Phys.*, **40**, 183–201 (1981).
22. U. Bulgareli, G. Graziani, D. Mansutti and R. Piva, 'A reduced implicit scheme, via discrete stream function generation, for unsteady Navier–Stokes equations in general curvilinear coordinates', *Proc. 6th GAMM Conf.*, Göttingen, 1986.
23. J. Burkhardt, C. Hall and T. Porsching, 'The dual variable method for the solution of compressible fluid flow problems', *SIAM J. Algeb. Discr. Methods*, **7**, 476–483 (1986).
24. S. H. Chou, 'A network model for incompressible two-fluid flow and its numerical solution', *Numer. Methods Partial Diff. Eqns*, **5**, 1–24 (1989).
25. A. E. Frey, C. A. Hall and T. A. Porsching, 'Numerical simulation of confined unsteady aerodynamical flows', *Int. j. numer. methods eng.*, **4**, 1233–1250 (1987).
26. J. W. Goodrich and W. Y. Soh, 'Time dependent viscous incompressible Navier–Stokes equations: the finite difference Galerkin formulations and stream function algorithms', *J. Comput. Phys.*, **79**, 113–134 (1988).
27. K. Gustafson and R. Hartman, 'Graph theory and fluid dynamics', *SIAM J. Algeb. Discr. Methods*, **6**, 643–656 (1985).
28. C. A. Hall, 'Numerical solution of Navier–Stokes problems by the dual variable method', *SIAM J. Algeb. Discr. Methods*, **6**, 220–236 (1985).
29. T. A. Porsching, 'A finite difference method for thermally expandable fluid transients', *Nucl. Sci. Eng.*, **64**, 177–186 (1977).
30. C. Berge and A. Ghouila-Houri, *Programming, Games and Transportation Networks*, Methuen, London, 1965.
31. D. J. Ewing, A. J. Fawkes and J. R. Griffiths, 'Rules governing the numbers of nodes and elements in a finite element mesh', *Int. j. numer. methods eng.*, **2**, 597–601 (1970).
32. I. P. Jones and C. P. Thompson, 'Numerical solutions for a comparison problem on natural convection in a closed cavity', *Tech. Rep. AERE-R9955*, Harwell, 1981.
33. A. B. Stephens, J. B. Bell, J. M. Solomon and L. B. Hackerman, 'A finite difference Galerkin formulation for the incompressible Navier–Stokes equations', *J. Comput. Phys.*, **53**, 152–172 (1984).